SCIENTIFIC REPORTS

OPEN

SUBJECT AREAS:
PROTEINS
X-RAY CRYSTALLOGRAPHY
SODIUM CHANNELS
ION CHANNELS IN THE NERVOUS SYSTEM

Received
5 June 2013

Accepted
29 July 2013

Published
14 August 2013

Correspondence and requests for materials should be addressed to J.S. (dbsjayar@nus.edu.sg)

Structural Basis for the Modulation of the Neuronal Voltage-Gated Sodium Channel $Na_V1.6$ by Calmodulin

Vishnu Priyanka Reddy Chichili[1], Yucheng Xiao[2], J. Seetharaman[3], Theodore R. Cummins[2] & J. Sivaraman[1]

[1]Department of Biological Sciences, National University of Singapore, Singapore, 117543, [2]Department of Pharmacology and Toxicology, Stark Neurosciences Research Institute, Indiana University School of Medicine, Indianapolis, IN, USA, [3]X4 Beamline, Brookhaven National Laboratory, Upton, New York, USA.

The neuronal-voltage gated sodium channel (VGSC), $Na_V1.6$, plays an important role in propagating action potentials along myelinated axons. Calmodulin (CaM) is known to modulate the inactivation kinetics of $Na_V1.6$ by interacting with its IQ motif. Here we report the crystal structure of *apo*-CaM:$Na_V1.6$IQ motif, along with functional studies. The IQ motif of $Na_V1.6$ adopts an α-helical conformation in its interaction with the C-lobe of CaM. CaM uses different residues to interact with $Na_V1.6$IQ motif depending on the presence or absence of Ca^{2+}. Three residues from $Na_V1.6$, Arg1902, Tyr1904 and Arg1905 were identified as the key common interacting residues in both the presence and absence of Ca^{2+}. Substitution of Arg1902 and Tyr1904 with alanine showed a reduced rate of $Na_V1.6$ inactivation in electrophysiological experiments *in vivo*. Compared with other CaM:Na_V complexes, our results reveal a different mode of interaction for CaM:$Na_V1.6$ and provides structural insight into the isoform-specific modulation of VGSCs.

Voltage-gated ion channels play a crucial role in the spread of action potentials by producing electrical signals in neurons and other excitable cells[1]. Voltage-gated sodium channels (VGSCs) are especially responsible for excitability in neuronal, neuroendocrine, skeletal muscle and cardiac cells. VGSCs are transmembrane proteins of approximately 260 kDa and consist of a central, pore-forming functional α subunit (VGSCα) and one or more auxiliary β subunits (VGSCβ)[2]. VGSCs are known to exist in three basic states: deactivated (closed), activated (open) and inactivated (closed). In the absence of external stimuli, VSGCs are found in the deactivated state and become opened (activated) upon receiving signals, which leads to the propagation of the action potential. Once activated, the VGSCs rapidly return to an inactivated state, during which another signal cannot be evoked[3]. Thus, activation and inactivation kinetics of VGSCs play a key role in normal nerve function and muscle contraction.

Among all the VGSCs, $Na_V1.1$, $Na_V1.2$ and $Na_V1.6$ are predominantly found in the central nervous system (CNS). $Na_V1.6$ channels are particularly crucial channels that exist at certain axonal sites, such as the nodes of Ranvier and axon initial segments (ISs), where action potentials are generated[4,5]. Proper function of $Na_V1.6$ is important since its loss or disruption in mice leads to symptoms of motor dysfunction, dystonia, paralysis, abnormalities in retinal pathways and even juvenile lethality[6,7]. A recent study on the differences between $Na_V1.1$, $Na_V1.2$ and $Na_V1.6$ has shown that $Na_V1.6$ channels are more suited for repetitive or high-frequency firing[8]. Repetitive firing is required when the postsynaptic and presynaptic regions of the neuron are separated by a few millimeters. In a study designed to investigate the role of $Na_V1.6$ in repetitive firing in Purkinje cells, it was shown that mice lacking $Na_V1.6$ channels exhibit loss of spontaneous firing, diminished repetitive firing abilities and cell degeneration[9]. Moreover, Herzog *et al.* reported that $Na_V1.6$ exhibits faster recovery from inactivation when compared with other VGSC isoforms, which helps in achieving repetitive firing[10]. Thus, $Na_V1.6$ plays an important role in propagating action potentials along the length of myelinated axons.

Calmodulin (CaM) is a ubiquitous protein that binds to many target proteins and regulates a number of cellular functions. CaM is known to interact with several of its binding partners via an isoleucine-glutamine (IQ) motif[11]. The general core region of the IQ motif is typically [I/L/V]QXXXRGXXX[R/K] and interactions mediated by IQ motifs can be either calcium-dependent or -independent[11]. The carboxyl terminus of all VGSC isoforms (Na_V 1.1–1.9) possesses an IQ motif that is conserved to various degrees and recognized by CaM. Indeed, several reports have shown that CaM is able to bind to and modulate the activation and steady-state inactivation of various VGSCs via this IQ motif in an isoform-dependent manner[12–19].

Mutations in the core region of $Na_V1.6$ IQ motif have been shown to cause reduced binding with CaM as well as reduced peak sodium current in the absence of Ca^{2+} [13]. Changes in the intracellular Ca^{2+} concentration are known to alter the inactivation kinetics of $Na_V1.6$ currents in a CaM-dependent mechanism[13]. Ca^{2+}/CaM has been shown to delay $Na_V1.6$ channel inactivation by 50% when compared with *apo*-CaM (Ca^{2+} free) induced rate of inactivation. Ca^{2+}/CaM-dependent slowing of $Na_V1.6$ inactivation kinetics could prolong action potential duration to enhance neurotransmitter release at nerve endings and thus regulate synaptic plasticity[13]. In order to determine how $Na_V1.6$ is regulated by CaM, it is necessary to understand the interaction between these two proteins.

In this study, we report the structural basis for the interaction of $Na_V1.6$IQ motif with CaM in the presence and absence of Ca^{2+}. The crystal structure of the *apo*-CaM-$Na_V1.6$ IQ motif complex revealed a different mode of interaction between CaM and $Na_V1.6$ IQ motif as compared with other CaM-Na_V IQ motif complexes. We also show that CaM employs different modes of interaction to bind the $Na_V1.6$ IQ motif in the presence and absence of Ca^{2+}, with enhanced affinity observed in the presence of Ca^{2+}. The crystal structure also revealed the importance of several key residues in mediating the interaction, and structure-based mutational studies were used to validate these interactions that were dependent on the presence and absence of Ca^{2+}. A comparison of the electrophysiological properties between these mutants and wild-type $Na_V1.6$ further validated the role of these interacting residues in modulating the inactivation kinetics of $Na_V1.6$.

Results

Sequence analysis. Sequence alignment of the IQ motifs of various isoforms of VGSCs reveals significant sequence similarity (Figure 1). The IQ motif of $Na_V1.6$ possesses Leu at position 1 of the IQ motif, whereas this position contains an Ile for the IQ motifs of the other isoforms. The $Na_V1.6$ IQ motif possesses Gly at position 7, whereas Arg is conserved at this position in many of the VGSC isoforms. This particular difference between IQ motifs has been known to represent two different functional classes of IQ domains[20]. About 50% of IQ domains are known to have a Gly residue at position 7 instead of bulky amino acid and this substitution may provide some specificity for CaM interactions[21]. To further understand the $Na_V1.6$ interaction with CaM, the $Na_V1.6$ IQ motif peptide was selected based on the analysis of structurally known CaM:IQ motif complexes[22]. This led us to select 1891–1914 aa of $Na_V1.6$ from *Mus musculus* as an appropriate $Na_V1.6$ IQ motif peptide for the biophysical interaction studies using ITC experiments.

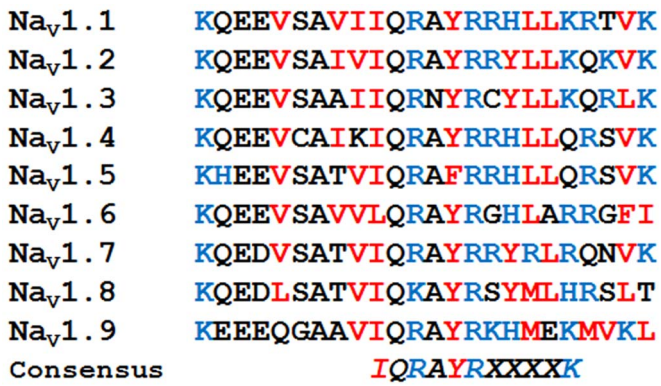

Figure 1 | Sequence alignment of the IQ motifs from various Na_V isoforms. Na_V IQ motifs comprise both hydrophobic (red) and positively charged (blue) amino acids that help in anchoring the IQ motif to CaM. 1891–1914 aa of $Na_V1.6$ are considered for further studies. This figure also shows the consensus sequence of the IQ motif region. For clarity, the Ile of IQ motif is numbered as position 1 in the consensus sequence.

Isothermal Titration Calorimetry (ITC). Interactions between CaM and the $Na_V1.6$ IQ motif peptide were studied in the presence and absence of Ca^{2+} (Table 1). The $Na_V1.6$ IQ motif peptide bound to CaM in a 1 : 1 ratio in the presence and absence of Ca^{2+} (Figure 2). The negative Gibbs free energy change for CaM-$Na_V1.6$ IQ interactions, in the presence and absence of Ca^{2+} indicated that all the interactions were thermodynamically favorable (Table 1). Moreover, the binding affinity for CaM with $Na_V1.6$ IQ motif peptide was enhanced in the presence of Ca^{2+}. It is possible that the mode of interaction between the IQ motif and CaM varies depending on the presence (Ca^{2+} bound) or absence (*apo*) of Ca^{2+} [23]. To better understand the structural basis for the difference in these interactions, we determined the crystal structure of CaM-$Na_V1.6$ IQ motif peptide complex.

Structure of *apo*-CaM-$(Gly)_5$-$Na_V1.6$ IQ motif peptide complex. Brief attempts to co-crystallize $Na_V1.6$ IQ motif peptide with CaM did not yield complex crystals. This led us to adopt the linker method, which has been described earlier[22,24–26]. Initially, residues 1891–1914 of $Na_V1.6$ were linked to the C-terminus of CaM using a $(Gly)_5$ linker. However, the crystals obtained were not of good quality. To optimize the fused construct, we instead used residues 1893–1914 of $Na_V1.6$ and obtained much better diffraction-quality crystals. The initial phases were obtained using SelMet-labeled crystals. The final model was refined with a native data set up to 1.95Å resolution with an R value of 0.201 (R_{free} = 0.236) (Table 2).

Our findings show that CaM exists in an extended conformation, with no electron density observed in any of the divalent metal ion binding sites. The helices of EF-hand motifs are parallel to each other, indicating the absence of Ca^{2+}. The electron density for residues 1893–1913 of $Na_V1.6$ IQ peptide is also well defined (Figure 3). Figure 4 shows that the bound $Na_V1.6$ IQ peptide assumes an α-helical structure and adopts an almost perpendicular orientation to the central helix of CaM, making several contacts with the C-lobe of CaM.

The C-lobe of CaM appears to be in a "semi-open" conformation, which would allow the IQ motif to interact. The N-lobe of CaM is not interacting with the IQ motif, remaining in a "closed" conformation. The interaction between CaM and $Na_V1.6$ IQ peptide is mainly electrostatic in nature. We identified the key residues of the $Na_V1.6$ IQ peptide involved in this interaction as Gln1901, Arg1902, Tyr1904, Arg1905, His1907 and Arg1911 (Figure 4). Leu1900 (at position 1) of the $Na_V1.6$ IQ motif peptide is buried in the hydrophobic cluster formed by Ile85, Phe89, Phe92, Leu105 and Met109 of CaM, with a buried area of 110 Å^2. The side-chain of Gln 1901 (position 2) has established hydrogen bonds with the main chain atoms of Met110, Leu113 and Glu115 of CaM, and is buried in the pocket formed by these interacting residues from CaM. Tyr1904 at position 5 is buried in the hydrophobic cluster formed by Leu116, Met125, Phe141 and Met146 from CaM, with a buried area of 139 Å^2. The hydroxyl group of Tyr1904 at position 5 forms a hydrogen bonding contact with Glu128 of CaM. Similarly, the side-chains of Arg1902, Arg1905, His1907 and Arg1911 from $Na_V1.6$ interact with the side-chains of Glu115, Glu121, Glu124 and Glu128 from CaM via hydrogen bonds. Altogether, $Na_V1.6$ IQ motif was shown to make14 hydrogen bond contacts (<3.2 Å) with the C-lobe of CaM (Supplementary Table 1).

Comparison with other CaM-Na_V IQ motif complexes. The NMR structures of *apo*-CaM C-lobe-$Na_V1.2$ IQ motif complex and *apo*-CaM-$Na_V1.5$ IQ motif complex have been reported[23,27]. The structure of the CaM-$Na_V1.6$ IQ motif peptide complex, particularly the C-lobe, was superimposed with the equivalent region of $Na_V1.2$ and $Na_V1.5$ IQ motif peptide complexes, with an

Table 1 | Thermodynamic parameters for interactions of the wild-type and mutants of CaM with the wild-type and various mutants of $Na_V1.6$ IQ motif peptide in the presence and absence of Ca^{2+}

		N	K_a (X10^6 M^{-1})	K_d (μM)	ΔH (kcal/mole)	TΔS (kcal/mole)	ΔG (kcal/mole)
apo-CaM	$Na_V1.6_{WT}$	0.95 ± 0.03	0.38 ± 0.04	2.63	−2.29 ± 0.12	5.33	−7.62
Ca^{2+}/CaM	$Na_V1.6_{WT}$	0.93 ± 0.02	0.63 ± 0.09	1.58	−6.87 ± 0.27	1.04	−7.91
apo-CaM	$Na_V1.6$ * Q1901A/R1902A/Y1904A/R1905A	-	-	-	-	-	-
Ca^{2+}/CaM	$Na_V1.6_{Q1901A}$	1.07 ± 0.02	0.47 ± 0.03	2.12	−4.88 ± 0.12	2.8	−7.7
	$Na_V1.6_{R1902A}$	1.02 ± 0.04	0.20 ± 0.02	5.00	−4.0 ± 0.21	3.2	−7.2
	$Na_V1.6_{Y1904A}$	1.05 ± 0.14	0.18 ± 0.05	5.55	−1.81 ± 0.33	5.3	−7.1
	$Na_V1.6_{R1905A}$	1.1 ± 0.06	0.25 ± 0.04	3.92	−2.49 ± 0. 20	4.9	−7.4
$Na_V1.6_{WT}$	*apo*-CaM * E115A/E121A/E124A/E128A	-	-	-	-	-	-
	Ca^{2+}/CaM_{E115A}	1.02 ± 0.02	0.72 ± 0.08	1.38	−4.9 ± 0.11	3.1	−8.0
	Ca^{2+}/CaM_{E121A}	0.98 ± 0.02	1.0 ± 0.13	1.00	−6.9 ± 0.13	1.2	−8.1
	Ca^{2+}/CaM_{E124A}	1.06 ± 0.02	0.71 ± 0.08	1.40	−6.9 ± 0. 2	1.0	−7.9
	Ca^{2+}/CaM_{E128A}	0.98 ± 0.02	0.56 ± 0.05	1.78	−6.4 ± 0.19	1.4	−7.8

Note: * No binding was observed for these single point amino acid substitutions.

rmsd of 1.3 Å and 0.76 Å for 59 and 58 Cα atoms, respectively. The interactions between the *apo*-C-lobe CaM and $Na_V1.2$ IQ motif complex were reported to be mainly hydrophobic in nature[23].

The one-to-one comparison of $Na_V1.2$ and $Na_V1.6$ IQ motif complex structures in the absence of Ca^{2+} is outlined in Figure 5A–C. It can be seen that the Arg residues at positions 3 and 6 of $Na_V1.6$ IQ motif make hydrogen bonding contacts with Glu115 and Glu121 of CaM, respectively (Figure 5A), whereas the same Arg residues of $Na_V1.2$ IQ motif do not interact with CaM (Figure 5B). Moreover, the orientation of the Tyr residues at position 5 of $Na_V1.6$ IQ motif and $Na_V1.2$ IQ motif are different; this is thought to allow the hydroxyl group of the Tyr residue in $Na_V1.6$ IQ motif to make hydrogen bonding contacts with Glu128 of CaM (Figure 5A); however, the same is not observed for the $Na_V1.2$ IQ motif (Figure 5B).

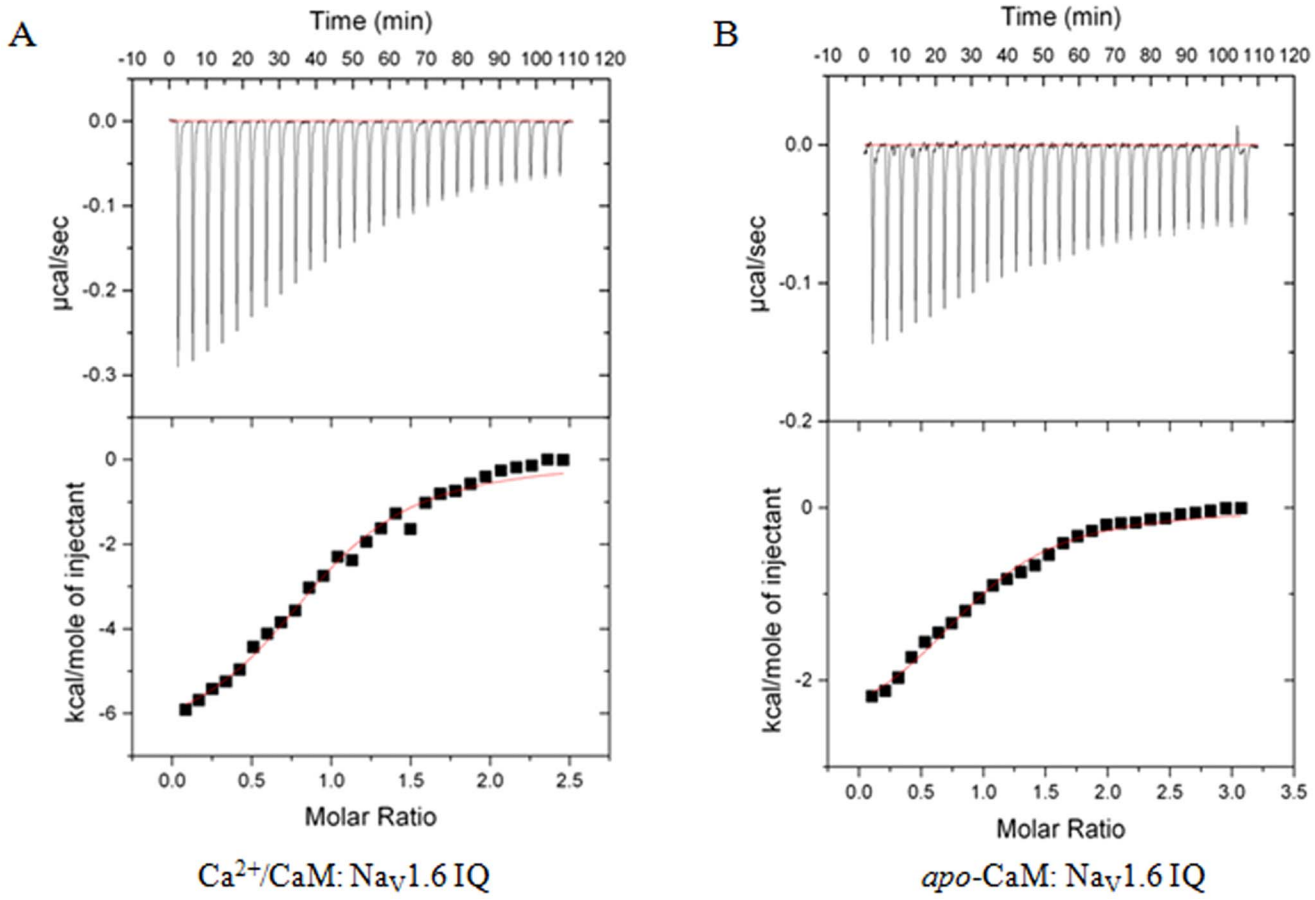

Figure 2 | ITC results for wild-type (WT) CaM with WT $Na_V1.6$ IQ motif peptides in the (A) presence and (B) absence of Ca^{2+}. All reactions were exothermic in nature and the upper panels show the raw ITC data for injection of IQ motif peptide into the sample cell containing CaM. The peaks were normalized to the peptide: protein molar ratio and were integrated as shown in the bottom panels. Solid dots indicate the experimental data, and their best fit was obtained from a non-linear least squares method, using a one-site binding model depicted by a continuous line.

Table 2 | Crystallographic data and refinement statistics for *apo*-CaM-$Na_V1.6$ IQ motif complex

	apo-CaM-$(Gly)_5$-$Na_V1.6$ IQ	
Data collection	Peak	Native
Cell parameters (Å, °)	a = 72.90, b = 50.76, c = 150.77 α = γ = 90, β = 91.6	a = 72.90, b = 50.76, c = 150.77 α = γ = 90, β = 91.5
Space group	$P2_1$	$P2_1$
Resolution range (Å) *	50.0 − 2.15 (2.23 − 2.15)	50.0 − 1.90 (1.93 − 1.90)
Wavelength (Å)	0.979	1.0
Observed reflections > 1σ	391779	518082
Unique reflections	57677	83450
Completeness (%)	93.9	94.9
Overall (I/σ (I))	28.6	37.5
R_{sym}[a] (%)	5.7	6.1
Refinement and quality [b]		
Resolution range (Å)		48.10 − 1.95 (2.00 − 1.95)
R_{work}[c] (no. of reflections)		0.201 (77108)
R_{free}[d] (no. of reflections)		0.236 (1828)
RMSD bond lengths (Å)		0.006
RMSD bond angles(°)		0.958
Average B-factorse (Å²)		
Main chain		36.6
Side chain		44.3
Ramachandran plot		
Most favored regions (%)		99.0
Allowed regions (%)		0.8
Disallowed regions (%)		0.2

[a]$R_{sym} = \sum |I_i - \langle I \rangle| / |I_i|$ where I_i is the intensity of the i^{th} measurement, and <I> is the mean intensity for that reflection.
[b]Reflections with I > σ was used in the refinement.
[c]$R_{work} = |F_{obs} - F_{calc}| / |F_{obs}|$ where F_{calc} and F_{obs} are the calculated and observed structure factor amplitudes, respectively.
[d]R_{free} = as for R_{work}, but for 5–7% of the total reflections chosen at random and omitted from refinement.
*The high resolution bin details are in the parenthesis.

The His residue at position 8 of $Na_V1.6$ IQ motif makes a hydrogen bonding contact with Glu128 of CaM, but this residue is replaced by a Tyr residue in the $Na_V1.2$ IQ motif, which is buried in the hydrophobic pocket formed by various hydrophobic residues of C-lobe of CaM; this causes the sidechain of Glu128 of CaM to be oriented away from the Tyr at position 8 of $Na_V1.2$ (Figure 5B).

The NMR structure of *apo*-CaM and $Na_V1.5$ IQ motif revealed an interaction mainly driven by hydrophobic forces and, to some extent, electrostatic interactions. Arg at position 3 of $Na_V1.5$ and $Na_V1.6$ IQ motif are involved in hydrogen bonding contact with CaM, but with different residues (Figure 5C). The Tyr at position 5 of $Na_V1.6$ IQ motif is replaced by Phe in the $Na_V1.5$ IQ motif, and has no hydrogen bonding contact with CaM (Figure 5C).

Structure-based mutational studies. Based on the crystal structure of CaM-$Na_V1.6$ IQ motif complex, we selected key interacting residues of CaM (Glu115, Glu121, Glu124, and Glu128) and $Na_V1.6$ IQ motif (Gln1901, Arg1902, Tyr1904, and Arg1905) and mutated them to alanine using site-directed mutagenesis. We then compared the binding of these unlinked CaM and $Na_V1.6$ IQ motifs using ITC to determine the importance of these key residues in mediating binding. We found that mutating any single residue either on CaM or $Na_V1.6$ IQ motif peptide abolished the binding in the absence of Ca^{2+}(Table 1 and Supplementary Figure 1). Similar losses of interaction between proteins and peptides have been previously reported following mutation of key interacting residues[28–31].

Next, we sought to examine the role of *apo*-CaM interacting residues of $Na_V1.6$ IQ motif in recognizing Ca^{2+}-bound CaM using ITC. We found that single mutations in the $Na_V1.6$ IQ motif peptide led to reduced binding with Ca^{2+}/CaM. Of the four $Na_V1.6$ mutants, Y1904A showed the most significant reduction in binding affinity (Table 1), followed by R1902A (Table 1 and Supplementary Figure 1). Since the conformation of CaM might be different in the presence of Ca^{2+}, it is likely that different residues would be exposed on the surface of CaM to interact with IQ motifs[32]. We therefore made brief attempts to crystallize Ca^{2+}/CaM-$Na_V1.6$ IQ motif peptide complex. However, we did not obtain any crystals. We then assessed the role of Ca^{2+} in regulating the interaction between mutated CaM and WT $Na_V1.6$ IQ motif in the presence of Ca^{2+}. These mutants of CaM did not show any reduction in binding affinity in the presence of Ca^{2+} (Table 1), suggesting that the $Na_V1.6$ IQ motif is recognized by different residues of CaM in the presence and absence of Ca^{2+}.

Reduced rate of inactivation by R1902A and Y1904A of $Na_V1.6$. Finally, we sought to compare the electrophysiological properties of mutating two key residues (R1902A and Y1904A) of $Na_V1.6$ channels with WT $Na_V1.6$ channels. Both WT and mutant channels were expressed in ND7/23 cells and studied under conditions of minimal (essentially zero) intracellular calcium. The two mutations significantly slowed the rate of the inactivation at potentials ranging from 0 to +40 mV (Figure 6A). At +20 mV, R1902A and Y1904A slowed the rate of fast inactivation of Nav1.6 channels by 31% and 48%, respectively. The slower rate of fast inactivation is not caused by the shift in the voltage dependence of channel gating. As can be seen in Supplementary Figure 2, neither R1902A nor Y1904A altered the steady-state activation of Nav1.6 channels. The two mutations also did not significantly alter the steady-state inactivation of $Na_V1.6$ channels (Supplementary Figure 2). Consistent with our previous finding that the IQ motif is an important determinant of current amplitude[13], the R1902A and Y1904A mutations decreased current density of $Na_V1.6$ channels by 42.4% and 73.8%, respectively (Figure 6B).

Discussion

The carboxy termini of VGSCs possess a CaM-binding IQ motif that is involved in the regulation of its inactivation kinetics (Supplementary Figure 3). Moreover, CaM is known to modulate the function of VGSCs in an isoform-dependent manner[12–19]. Disruption of CaM-mediated VGSC regulation through mutations in the IQ motif results in abnormalities linked to life-threatening idiopathic ventricular arrhythmias in cardiac muscle and various other disorders[17,33–35]. The aim of the present study was to understand the interactions between CaM and the IQ motif of $Na_V1.6$, a VGSC involved in the propagation of action potentials along myelinated axons in the central nervous system.

Ca^{2+} plays a crucial role in CaM mediated regulation of VGSCs. It is known that Ca^{2+}/CaM mediates slow inactivation and *apo*-CaM mediates fast inactivation observed in the electrophysiological studies of several VGSCs interacting via their IQ motifs, $Na_V1.4$, $Na_V1.5$ and $Na_V1.6$[13,15,17,18]. We have observed that the IQ motif of $Na_V1.6$ has a higher affinity towards Ca^{2+}/CaM than *apo*-CaM. However, it is known that the IQ motif of cardiac muscle VGSC, $Na_V1.5$, shows a higher affinity towards *apo*-CaM than Ca^{2+}/CaM[15] (Table 3). The isoform-specific differences in terms of binding affinity and how this

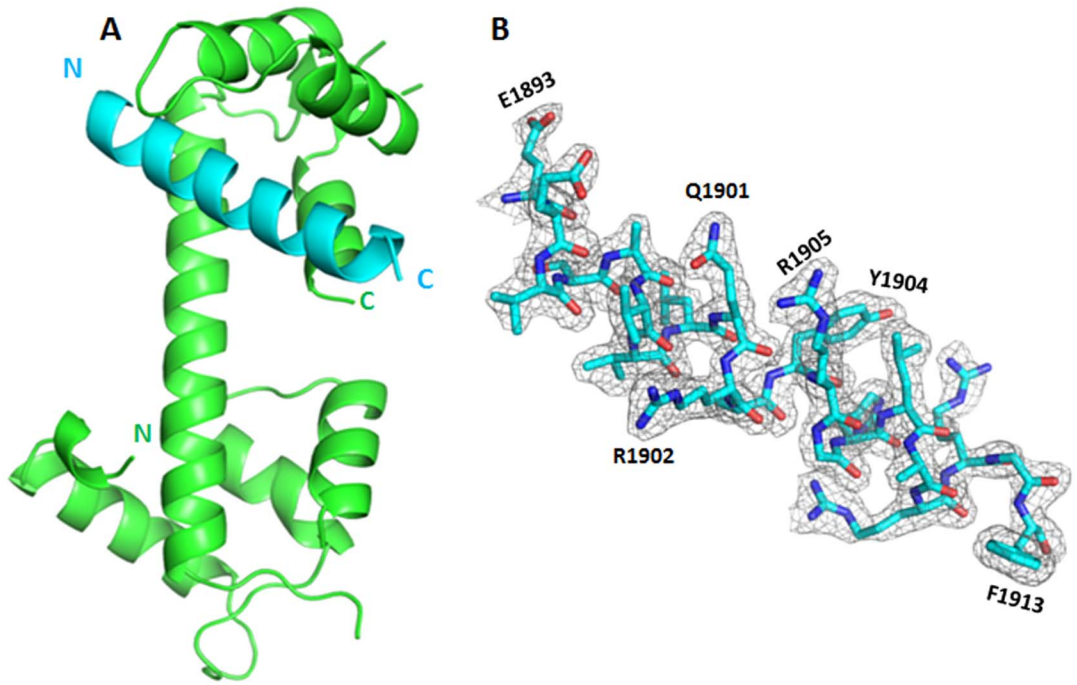

Figure 3 | Crystal structure of *apo*-CaM-$(Gly)_5$-$Na_V1.6$ IQ peptide complex. (A) Ribbon representation of *apo*-CaM-$(Gly)_5$-$Na_V1.6$ IQ peptide complex, where $Na_V1.6$ IQ peptide (cyan) is shown to be interacting with the C-lobe of CaM (green). The N- and C-terminus of CaM and $Na_V1.6$ IQ peptide are labeled. CaM interacting $Na_V1.6$ IQ peptide is derived from the symmetry related molecule. (B) 2Fo-Fc map of $Na_V1.6$ IQ peptide at a map contour level of 1σ. Terminal residues (E1893 and F1913) and key interacting residues of $Na_V1.6$ IQ peptide are labeled.

affects Ca^{2+}/CaM and *apo*-CaM-mediated inactivation may depend on the cellular localization of the respective VGSCs.

Although $Na_V1.2$ and $Na_V1.6$ are expressed in the CNS, they are known to exhibit different electrophysiological properties, including the amount of Na^+ current, as well as the onset of and recovery from inactivation[36,37]. $Na_V1.2$ and $Na_V1.6$ are necessary to propagate action potentials along the length of the unmyelinated and myelinated axons in the CNS, respectively. $Na_V1.2$ and $Na_V1.6$ are known to undergo fast inactivation via its C-terminus in the absence of Ca^{2+} [13,38]. However, there are a few differences between the two isoforms that have been highlighted. For instance, $Na_V1.6$ is more suitable for repetitive firing than $Na_V1.2$[8]. One study showed that the high affinity (nM K_d) between CaM and $Na_V1.2$ IQ motif would promote constitutive binding of CaM to $Na_V1.2$ IQ motif, independent of intracellular Ca^{2+} levels[23] (Table 3). In the present study, we observed moderate affinity (μM K_d) between CaM and the $Na_V1.6$ IQ motif in the presence and absence of Ca^{2+}. Thus, this difference in binding affinity exhibited by CaM towards $Na_V1.2$ and $Na_V1.6$ IQ motifs could dictate the functional properties of the respective VGSCs.

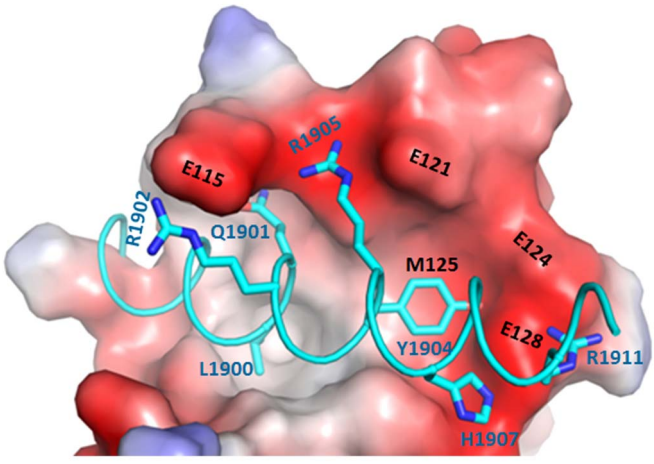

Figure 4 | Key interactions between CaM and $Na_V1.6$ IQ peptide complex. CaM is shown in electrostatic surface representation and key residues involved in the interaction are labeled in black. Red represents negative potential and blue represents positive potential. Important residues of $Na_V1.6$ IQ peptide involved in the interaction are shown as sticks and are labeled in cyan.

The crystal structure of the *apo*-CaM-$Na_V1.6$ IQ motif peptide complex showed that the interaction is mediated by the C-lobe of CaM. CaM-$Na_V1.6$ IQ motif complex has been obtained by linking the IQ motif peptide to the C-terminus of CaM using a $(Gly)_5$ linker. In the complex crystal structure, instead of having intramolecular interactions between CaM and $Na_V1.6$ IQ peptide, we have observed intermolecular interactions such that the IQ peptide fused with one CaM molecule is interacting with the nearby symmetry related (adjacent) CaM molecule. Similar intermolecular interactions have been previously reported[22,24,39]. In the core "IQ" region of $Na_V1.6$, mutations of LQ to LE and EE are known to result in reduced binding with CaM. In particular, the EE mutant slows $Na_V1.6$ inactivation by 48% by affecting its interaction with *apo*-CaM[13]. In our report, the crystal structure of *apo*-CaM-$Na_V1.6$ IQ motif complex revealed that Leu1900 at position 1 is buried in the hydrophobic cluster of CaM residues, and thus replacing it with a negatively charged residue such as Glu may affect the interaction. Indeed, substitution of Gln1901 with Glu affected *apo*-CaM mediated fast inactivation, but did not result in a complete loss of this affect[13]. Despite this, we observed a complete loss of interaction between $Na_V1.6$ IQ motif and *apo*-CaM in our ITC experiments when Gln1901 was mutated to Ala.

Our structure-guided mutational studies demonstrated that Arg1902, Tyr1904 and Arg1905 of the $Na_V1.6$ core IQ motif region are not only important for its interaction with *apo*-CaM but also for that with Ca^{2+}/CaM. In particular, the Y1904A substitution abolishes the interaction between $Na_V1.6$ IQ motif and *apo*-CaM and, reduces affinity to a large extent towards Ca^{2+}/CaM. R1902A also decreased

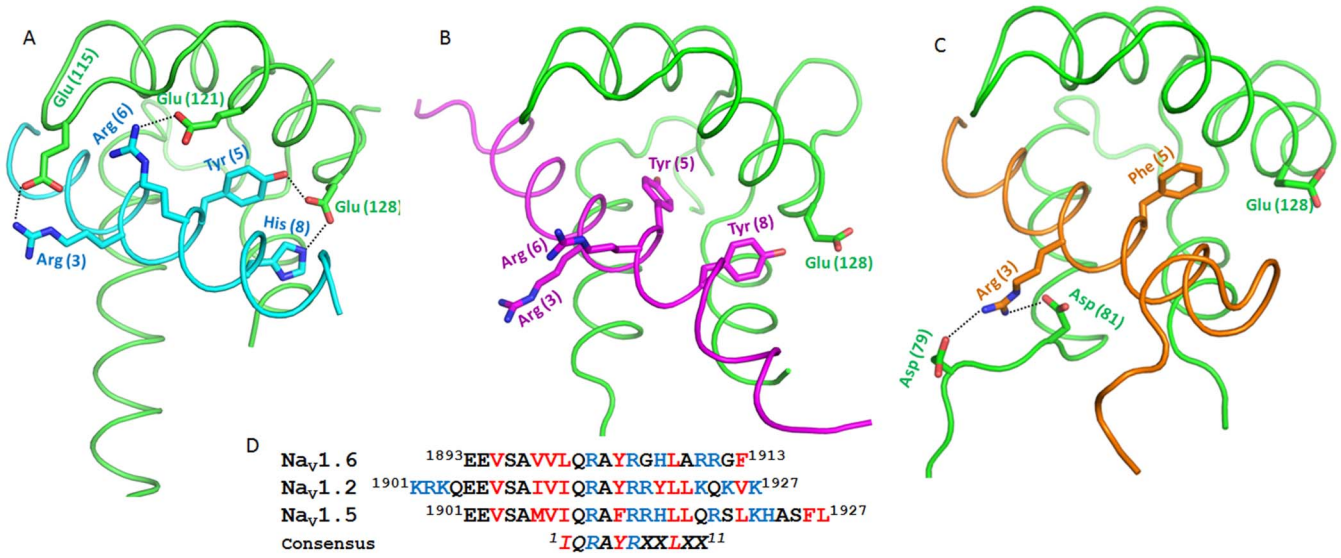

Figure 5 | Differences in the interactions between CaM and various Na_V isoforms: (A) Crystal structure of *apo*-CaM-Na_V1.6 IQ motif complex, and NMR structures of (B) *apo*-CaM-Na_V1.2 IQ motif complex (PDB 2KXW) and (C) *apo*-CaM-Na_V1.5 IQ motif complex (PDB 2L53). Sidechains of Na_V1.6 (cyan), Na_V1.2 (magenta) and Na_V1.5 (orange) IQ motifs and CaM (green) are highlighted as sticks and selected hydrogen bonds involved are shown as black dashed lines. Positions of the residues are given in parentheses. (D) Structure based sequence alignment of structurally known IQ motif peptides from Na_V1.6, Na_V1.2 and Na_V1.5 in complex with *apo*-CaM. Similar to Figure 1, the consensus sequence of the IQ motif region is shown, and the Ile of IQ motif is numbered as position 1.

the interaction with both forms of CaM. Importantly, channels containing these mutations showed reduced rates of inactivation and current density as compared with their wild-type counterpart (in the absence of Ca^{2+}), further confirming the importance of these residues. We also observed that the residues of CaM involved in its interaction with Na_V1.6 IQ motif are different in the presence and absence of Ca^{2+}. Although E115A, E121A, E124A and E128A mutants of CaM showed no reduction in binding with Na_V1.6 IQ motif in the presence of Ca^{2+}, the E115A mutant of Ca^{2+}/CaM showed reduced enthalpy and increased entropy as compared with the wild-type interaction. This enthalpy-entropy compensation suggests a loss of key interaction in the bound state and is compensated by increased disorder[40,41]. Thus, Glu115 of CaM could be involved in the interaction with Na_V1.6 IQ motif, whereas the other residues (Glu121, Glu124 and Glu128 of CaM) are not involved in the interaction in the presence of Ca^{2+}.

Although the structures of *apo*-CaM in complex with Na_V1.2 and Na_V1.5 IQ motif were similar to that observed with Na_V1.6 IQ motif, the sidechain interactions of the IQ motifs were different for each case. Moreover, *in silico* alanine-scanning mutagenesis of *apo*-CaM-Na_V1.5 IQ motif complex revealed that none of the residues from CaM provide the greatest contribution for the interaction, possibly due to the large number of CaM residues involved in creating the binding interface[27]. The mutational studies based on *apo*-CaM-Na_V1.6 IQ motif complex revealed that substituting a single interacting residue of CaM with Ala resulted in complete loss of interaction with Na_V1.6 IQ motif. This could probably explain why the interactions of *apo*-CaM-Na_V1.2 IQ motif and *apo*-CaM-Na_V1.5 IQ motif exhibit lower dissociation constants (K_d) than that of *apo*-CaM-Na_V1.6 IQ motif (Table 3). The binding of CaM to the IQ motif of Na_V1.8 VGSC is involved in recovery from inactivation[42]. However, the mutants R1902A and Y1904A of Na_V1.6 did not show any significant difference in the recovery from inactivation (Supplementary Figure 2). It is possible that the inactivation and recovery from inactivation properties of Na_V1.6 and Na_V1.8 are quite different. However, our data does not rule out the possibility that CaM might modulate recovery from slow inactivation for Na_V1.6 channels.

In summary, our studies reveal that the Na_V1.6 IQ motif has a relatively lower affinity towards CaM as compared with Na_V1.2 IQ

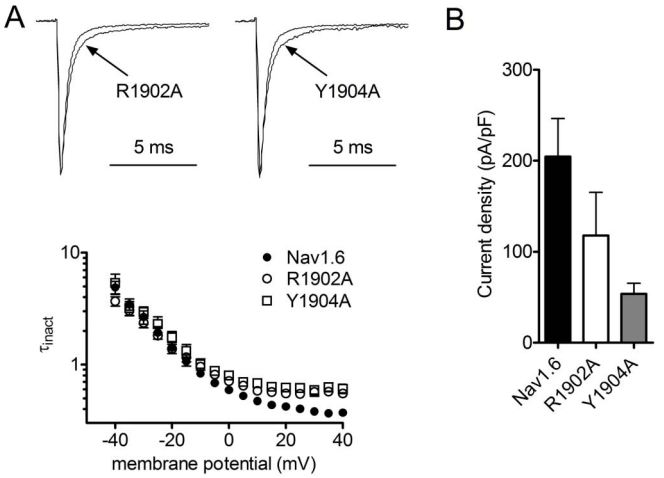

Figure 6 | Electrophysiological properties of mutant Na_V1.6 channels. (A) The two mutations R1902A and Y1904A altered the inactivation kinetics of Na_V1.6 channels. *Upper*, representative current traces of wild-type (WT), R1902A and Y1904A channels were elicited by a depolarizing potential of +20 mV. *Lower*, inactivation time constants as a function of voltage. The inactivation time constant is greater for Na_V1.6 R1902A currents (open circles; n = 11) than for Na_V1.6 WT currents (filled circles; n = 11) at all voltages ranging from 0 to +40 mV (Student's *t* test, $p < 0.05$). The inactivation time constant is greater for Na_V1.6 Y1904 currents (open squares; n = 10) than for Na_V1.6 WT currents at all voltages ranging from −5 to +40 mV ($p < 0.05$). Inactivation time constants were determined by Hodgkin & Huxley fits to the currents elicited by 50-ms depolarizing steps to the indicated potential. (B) The mutant Y1904A channels produce significantly lower peak current density than Na_V1.6 WT channels. Families of sodium currents of Nav1.6 WT, R1902 and Y1904 channels were elicited by 50-ms depolarizing steps to various potentials ranging from −80 to +40 mV. The maximum amplitude of peak currents was divided by cell capacitance.

Table 3 | Comparison of various properties of different VGSC isoforms

VGSC	Location	IQ motif:CaM affinity (K_d)		Inactivation		
		In the presence of Ca^{2+}	In the absence of Ca^{2+}	In the presence of Ca^{2+}	In the absence of Ca^{2+}	Recovery from inactivation in the absence of Ca^{2+}
$Na_V1.6$	Neurons (myelinated axons)	1.58 μM (present study)	2.63 μM (present study)	Slow (Ref 13)	Fast (Ref 13)	Faster than $Na_V1.7$ and $Na_V1.2$ (Ref 10, 37)
$Na_V1.2$	Neurons (unmyelinated axons)	≤10 nM (Ref 23)	≤10 nM (Ref 23)	N/A	Fast (Ref 38)	Fast (Ref 36)
$Na_V1.5$	Cardiac muscle	6.45 μM (Ref 15)	0.34 μM (Ref 15)	Slow (Ref 17)	Fast (Ref 17)	Fast

N/A- Not available.

motif, which provides a basis for the differences in the properties exhibited by these two neuronal VGSCs. Moreover, $Na_V1.5$ and $Na_V1.6$ IQ motifs show differences in affinity towards Ca^{2+}/CaM or *apo*-CaM, suggesting that the affinity of the Na_V IQ motif and CaM is different between cardiac and neuronal VGSCs. In the *apo*-CaM-$Na_V1.6$ IQ motif complex structure, we show that the C-lobe of CaM is in a semi-open conformation and its interactions with $Na_V1.6$ IQ motif are mediated by hydrogen bonds and hydrophobic contacts. Furthermore, ITC experiments identified Tyr1904 as a key residue for the interaction of $Na_V1.6$ IQ motif with both *apo*- and Ca^{2+}/CaM. The electrophysiological experiments confirmed the role of these key interacting residues in modulating the inactivation kinetics of $Na_V1.6$ channel. In addition, $Na_V1.6$ IQ motif adopts a different mechanism of interaction with *apo*-CaM compared to other known CaM-Na_V complex structures. Overall, these findings provide additional molecular insight into the isoform-specific regulation of VGSCs by CaM.

Methods

Cloning, expression and purification of CaM constructs. CaM was cloned into MCS1 cloning site (between BamHI and SalI restriction sites) of the pETDuet-1 (Novagen, Madison, WI) expression vector. $Na_V1.6$IQ motif (1893–1914) was linked to the C-terminus of CaM via a 5-glycine flexible linker (CaM-$(Gly)_5$-$Na_V1.6$ IQ) using a three-step fusion PCR procedure, as described by Ye *et al*[43]. The final PCR product was digested with NdeI and XhoI restriction enzymes (New England Biolabs, Ips wich, MA) along with the pGS21a vector (GeneScript, Piscataway, NJ). Predigested CaM-$(Gly)_5$-$Na_V1.6$ IQ gene and pGS21a vector were ligated, transformed into chemically competent *E. coli* DH5α cells and screened for positive colonies.

For protein expression, recombinant plasmids were transformed into *E. coli* BL21 (DE3) competent cells and cultured in 1 L LB media (supplemented with 100 μg/mL ampicillin) at 37°C until the OD_{600} reached between 0.6–0.8 AU. Protein expression was induced with 0.15 mM IPTG for 16 h at 16°C. Cell pellets were resuspended in 50 ml of lysis buffer (50 mM TrisHCl pH 7.4, 200 mM NaCl, 5% glycerol, 5 mM imidazole, 10 mM β-mercaptoethanol and 1 ml of protease inhibitor cocktail (Sigma-Aldrich, St. Louis, MO)). The cell suspension was sonicated and then centrifuged at 39,000 xg for 30 min. The supernatant was mixed with 5 ml of Ni-NTA resin (Qiagen, Valencia, CA) pre-equilibrated with lysis buffer for 1 hr. Resin was washed 3 times with lysis buffer and the bound proteins were eluted using 10 ml of lysis buffer supplemented with 500 mM imidazole. Eluted proteins were passed on to HiLoad 16/60 Superdex™ 75 prep grade (GE Healthcare, Buckinghamshire, UK) and eluted in one of two solutions comprising 50 mM TrisHCl pH 7.4 with 1 mM $CaCl_2$ (solution 1) or 50 mM TrisHCl pH 7.4, 1 mM EGTA (solution 2). In order to facilitate structure determination by heavy atom phasing, the Seleno-L-methionine labeled proteins were produced using M9 media, and proteins were purified by adopting a similar protocol, as mentioned above. All protein purification steps were carried out at 4°C.

Isothermal titration calorimetry. Binding affinities between $Na_V1.6$ IQ motifs (1891–1914) and Ca^{2+}/CaM or *apo*-CaM were studied using isothermal titration calorimetry (ITC). All peptides used in this study were purchased from GL Biochem Ltd (Shanghai, China). All proteins/peptides were dialyzed with buffer consisting of 50 mM Tris HCl (pH 7.4), 100 mM NaCl and 1 mM $CaCl_2$ for Ca^{2+}/CaM interaction studies, and 50 mM Tris HCl (pH 7.4), 100 mM NaCl and 1 mM EGTA for *apo*-CaM interaction studies. ITC experiments were performed using VP-ITC calorimeter (Microcal, LLC, Northampton, MA) at 25°C with 0.3 ml of 120–150 μM of $Na_V1.6$IQ motif peptides in the syringe and 1.4 ml of 10 μM of Ca^{2+}/CaM or *apo*-CaM in the sample cell. All the samples were thoroughly degassed and centrifuged to remove any precipitates. Volumes of 10 μl per injection were used for all experiments and consecutive injections were separated by 4 min to allow the peak to return to baseline. ITC data were analyzed with a single-site fitting model using Origin 7.0 software (OriginLab Corp., Northampton, MA).

Crystallization and structure determination. Crystallization screening for *apo*-CaM-$(Gly)_5$-$Na_V1.6$ IQ complexes were performed with a concentration of 18 mg/ml using the Hanging drop vapor diffusion method at room temperature. The initially identified condition from Hampton Research (Aliso Viejo, CA) was further optimized and the best crystals for *apo*-CaM-$(Gly)_5$-$Na_V1.6$ IQ were obtained from a condition consisting of 0.1 M Bis-Tris propane pH 7.0 and 56% Tacsimate. Where necessary, crystals were cryo-protected with 70% Tacsimate and flash-cooled in N_2 cold stream at 100 K.

The *apo*-CaM-$(Gly)_5$-$Na_V1.6$ IQ crystallized in the $P2_1$ space group and had four molecules in the asymmetric unit. Complete SAD (Single wavelength Anomalous Dispersion) data sets were collected at X6A beam line, NSLS, Brookhaven National Laboratory using a Quantum 4-CCD detector (Area Detector Systems Corp Poway, CA). All data sets were collected at 100 K. Data sets were indexed, integrated and scaled using HKL2000[44]. Heavy atom (Se) location, phasing and density modification was performed using Phenix Autosol[45]. Model building was carried out using Phenix Autobuild[45]. Where required, the protein model was manually built using the program COOT[46] and refinement was performed using Phenix Refine[45]. When the R-factors were less than 30%, well-ordered water molecules were added. The model has good stereochemistry, with all the residues within the allowed region of Ramachandran plot, as analyzed by PROCHECK[47]. All structure-related figures reported in this paper were generated using PyMol[48].

Site directed mutagenesis. Site-directed mutagenesis on CaM gene was achieved via inverse PCR technique[49] using the KapaHiFi DNA polymerase Kit (KAPA Biosystems, MA). Linear gene products were gel extracted and transformed into *E. coli* DH5αcells. Positive plasmids were transformed into *E. coli* BL21 (DE3) competent cells for protein expression, as described earlier.

Plasmid and construction of Nav1.6 mutants. The cDNA encoding a TTX-resistant mouse Nav1.6 construct was subcloned into a modified pcDNA3.1 vector, as described previously[13]. All mutations were introduced into the TTX-resistant mNav1.6 cDNA construct using the QuikChange II XL site-directed mutagenesis kit (Agilent Technologies, Inc., Santa Clara, CA) according to the manufacturer's instruction. The constructs were sequenced to confirm that the appropriate mutations were made.

Electrophysiology experiments. WT and mutant mNav1.6 channels were transiently transfected into ND7/23 cells using the standard calcium phosphate precipitation method, as previously described[13]. Whole-cell patch-clamp recordings were performed at room temperature (approximately 21°C) using an EPC-10 amplifier (HEKA, Lambrecht, Germany). Fire-polished electrodes were fabricated from 1.7-mm capillary glass (VWR, West Chester, PA) using a P-97 puller (Sutter, Novato, CA). The standard pipette solution contained 140 mM CsF, 1 mM EGTA, 10 mM NaCl, and 10 mM HEPES, pH 7.3. The standard bathing solution was 140 mM NaCl, 3 mM KCl, 1 mM $MgCl_2$, 1 mM $CaCl_2$, and 10 mM HEPES, pH 7.3. After filling with pipette solution, the access resistance of the electrode pipette ranged from 1.2 to 1.6 MΩ. The liquid junction potential for these solutions was <8 mV; data were not corrected to account for this offset. Voltage errors were minimized using 70–90% series resistance compensation, and the capacitance artifact was canceled using the computer-controlled circuitry of the patch clamp amplifier. Linear leak subtraction, based on resistance estimates from four to five hyperpolarizing pulses applied before the depolarizing test potential, was used for all voltage clamp recordings. Membrane currents were usually filtered at 5 kHz and sampled at 20 kHz. All cells were held at −100 mV for 5 min before the measurement of sodium currents. In order to avoid contamination from endogenous ND7/23 sodium currents, the currents of the TTX-resistant constructs were recorded in the presence of 500 nM TTX.

Protein data bank accession code. Coordinates and structure factors of *apo*-CaM-$(Gly)_5$-$Na_V1.6$ IQ have been deposited with RCSB Protein Data Bank with code 3WFN.

1. Barnett, M. W. & Larkman, P. M. The action potential. *Pract Neurol* **7**, 192–7 (2007).

2. Yu, F. H. & Catterall, W. A. Overview of the voltage-gated sodium channel family. *Genome Biol* **4**, 207 (2003).
3. Yellen, G. The moving parts of voltage-gated ion channels. *Q Rev Biophys* **31**, 239–95 (1998).
4. Caldwell, J. H., Schaller, K. L., Lasher, R. S., Peles, E. & Levinson, S. R. Sodium channel Na(v)1.6 is localized at nodes of ranvier, dendrites, and synapses. *Proc Natl Acad Sci U S A* **97**, 5616–20 (2000).
5. Boiko, T. *et al.* Functional specialization of the axon initial segment by isoform-specific sodium channel targeting. *J Neurosci* **23**, 2306–13 (2003).
6. Van Wart, A. & Matthews, G. Impaired firing and cell-specific compensation in neurons lacking nav1.6 sodium channels. *J Neurosci* **26**, 7172–80 (2006).
7. Smith, B. J. & Cote, P. D. Reduced Retinal Function in the Absence of Na(v)1.6. *PLoS One* **7**, e31476 (2012).
8. Zhou, W. & Goldin, A. L. Use-dependent potentiation of the Nav1.6 sodium channel. *Biophys J* **87**, 3862–72 (2004).
9. Raman, I. M., Sprunger, L. K., Meisler, M. H. & Bean, B. P. Altered subthreshold sodium currents and disrupted firing patterns in Purkinje neurons of Scn8a mutant mice. *Neuron* **19**, 881–91 (1997).
10. Herzog, R. I., Cummins, T. R., Ghassemi, F., Dib-Hajj, S. D. & Waxman, S. G. Distinct repriming and closed-state inactivation kinetics of Nav1.6 and Nav1.7 sodium channels in mouse spinal sensory neurons. *J Physiol* **551**, 741–50 (2003).
11. Bahler, M. & Rhoads, A. Calmodulin signaling via the IQ motif. *FEBS Lett* **513**, 107–13 (2002).
12. Gaudioso, C. *et al.* Calmodulin and calcium differentially regulate the neuronal Nav1.1 voltage-dependent sodium channel. *Biochem Biophys Res Commun* **411**, 329–34 (2011).
13. Herzog, R. I., Liu, C., Waxman, S. G. & Cummins, T. R. Calmodulin binds to the C terminus of sodium channels Nav1.4 and Nav1.6 and differentially modulates their functional properties. *J Neurosci* **23**, 8261–70 (2003).
14. Shah, V. N. *et al.* Calcium-dependent regulation of the voltage-gated sodium channel hH1: intrinsic and extrinsic sensors use a common molecular switch. *Proc Natl Acad Sci U S A* **103**, 3592–7 (2006).
15. Sarhan, M. F., Tung, C. C., Van Petegem, F. & Ahern, C. A. Crystallographic basis for calcium regulation of sodium channels. *Proc Natl Acad Sci U S A* **109**, 3558–63 (2012).
16. Deschenes, I. *et al.* Isoform-specific modulation of voltage-gated Na(+) channels by calmodulin. *Circ Res* **90**, E49–57 (2002).
17. Tan, H. L. *et al.* A calcium sensor in the sodium channel modulates cardiac excitability. *Nature* **415**, 442–7 (2002).
18. Young, K. A. & Caldwell, J. H. Modulation of skeletal and cardiac voltage-gated sodium channels by calmodulin. *J Physiol* **565**, 349–70 (2005).
19. Biswas, S. *et al.* Calmodulin regulation of Nav1.4 current: role of binding to the carboxyl terminus. *J Gen Physiol* **131**, 197–209 (2008).
20. Black, D. J., LaMartina, D. & Persechini, A. The IQ domains in neuromodulin and PEP19 represent two major functional classes. *Biochemistry* **48**, 11766–72 (2009).
21. Terrak, M., Wu, G., Stafford, W. F., Lu, R. C. & Dominguez, R. Two distinct myosin light chain structures are induced by specific variations within the bound IQ motifs-functional implications. *EMBO J* **22**, 362–71 (2003).
22. Kumar, V. *et al.* Structural basis for the interaction of unstructured neuron specific substrates neuromodulin and neurogranin with calmodulin. *Sci Rep* **3**, 1392 (2013).
23. Feldkamp, M. D., Yu, L. & Shea, M. A. Structural and energetic determinants of apo calmodulin binding to the IQ motif of the Na(V)1.2 voltage-dependent sodium channel. *Structure* **19**, 733–47 (2011).
24. Reddy Chichili, V. P., Kumar, V. & Sivaraman, J. Linkers in the structural biology of protein-protein interactions. *Protein Sci* **22**, 153–67 (2013).
25. Chichili, V. P. R., Kumar, V. & Sivaraman, J. A Protocol to Retain Weakly Interacting Protein Complexes for Structural Studies using an Appropriate Linker. *Protocol Exchange*, doi:10.1038/protex.2013.062 (2013).
26. Chichili, V. P. R., Kumar, V. & Sivaraman, J. A method to trap transient and weak interacting protein complexes for structural studies. *Intrinsically Disordered Proteins* 1,e25464 (2013).
27. Chagot, B. & Chazin, W. J. Solution NMR structure of Apo-calmodulin in complex with the IQ motif of human cardiac sodium channel NaV1.5. *J Mol Biol* **406**, 106–19 (2011).
28. McFarland, B. J., Katz, J. F., Sant, A. J. & Beeson, C. Energetics and cooperativity of the hydrogen bonding and anchor interactions that bind peptides to MHC class II protein. *J Mol Biol* **350**, 170–83 (2005).
29. Bridges, K. G., Chow, C. S. & Coen, D. M. Identification of crucial hydrogen-bonding residues for the interaction of herpes simplex virus DNA polymerase subunits via peptide display, mutational, and calorimetric approaches. *J Virol* **75**, 4990–8 (2001).
30. Rainsford, E. W., Harouaka, D. & Wertz, G. W. Importance of hydrogen bond contacts between the N protein and RNA genome of vesicular stomatitis virus in encapsidation and RNA synthesis. *J Virol* **84**, 1741–51 (2010).
31. Sant, A. J. *et al.* Individual hydrogen bonds play a critical role in MHC class II: peptide interactions: implications for the dynamic aspects of class II trafficking and DM-mediated peptide exchange. *Immunol Rev* **172**, 239–53 (1999).
32. Dash, S., Niemaczura, W. & Harrington, H. M. Characterization of the basic amphiphilic alpha-helix calmodulin-binding domain of a 61.5 kDa tobacco calmodulin-binding protein. *Biochemistry* **36**, 2025–9 (1997).
33. Veldkamp, M. W. *et al.* Two distinct congenital arrhythmias evoked by a multidysfunctional Na(+) channel. *Circ Res* **86**, E91–7 (2000).
34. Wang, D. W., Makita, N., Kitabatake, A., Balser, J. R. & George, A. L., Jr. Enhanced Na(+) channel intermediate inactivation in Brugada syndrome. *Circ Res* **87**, E37–43 (2000).
35. Weiss, L. A. *et al.* Sodium channels SCN1A, SCN2A and SCN3A in familial autism. *Mol Psychiatry* **8**, 186–94 (2003).
36. Rush, A. M., Dib-Hajj, S. D. & Waxman, S. G. Electrophysiological properties of two axonal sodium channels, Nav1.2 and Nav1.6, expressed in mouse spinal sensory neurones. *J Physiol* **564**, 803–15 (2005).
37. O'Leary, M. E. Characterization of the isoform-specific differences in the gating of neuronal and muscle sodium channels. *Can J Physiol Pharmacol* **76**, 1041–50 (1998).
38. Mantegazza, M., Yu, F. H., Catterall, W. A. & Scheuer, T. Role of the C-terminal domain in inactivation of brain and cardiac sodium channels. *Proc Natl Acad Sci U S A* **98**, 15348–53 (2001).
39. Kingston, R. L., Hamel, D. J., Gay, L. S., Dahlquist, F. W. & Matthews, B. W. Structural basis for the attachment of a paramyxoviral polymerase to its template. *Proc Natl Acad Sci U S A* **101**, 8301–6 (2004).
40. Dunitz, J. D. Win some, lose some: enthalpy-entropy compensation in weak intermolecular interactions. *Chem Biol* **2**, 709–12 (1995).
41. Van Petegem, F., Chatelain, F. C. & Minor, D. L., Jr. Insights into voltage-gated calcium channel regulation from the structure of the CaV1.2 IQ domain-Ca2+/calmodulin complex. *Nat Struct Mol Biol* **12**, 1108–15 (2005).
42. Choi, J. S., Hudmon, A., Waxman, S. G. & Dib-Hajj, S. D. Calmodulin regulates current density and frequency-dependent inhibition of sodium channel Nav1.8 in DRG neurons. *J Neurophysiol* **96**, 97–108 (2006).
43. Ye, Q., Li, X., Wong, A., Wei, Q. & Jia, Z. Structure of calmodulin bound to a calcineurin peptide: a new way of making an old binding mode. *Biochemistry* **45**, 738–45 (2006).
44. Otwinowski, Z. & Minor, W. Processing of X-ray diffraction data collected in oscillation mode. *Macromolecular Crystallography, Pt A* **276**, 307–326 (1997).
45. Adams, P. D. *et al.* PHENIX: a comprehensive Python-based system for macromolecular structure solution. *Acta Crystallogr D Biol Crystallogr* **66**, 213–21 (2010).
46. Emsley, P. & Cowtan, K. Coot: model-building tools for molecular graphics. *Acta Crystallogr D Biol Crystallogr* **60**, 2126–32 (2004).
47. Laskowski, R. A., Macarthur, M. W., Moss, D. S. & Thornton, J. M. PROCHECK: a program to check the stereochemical quality of protein structures. *Journal of Applied Crystallography* **26**, 283–291 (1993).
48. DeLano, W. L. & Lam, J. W. PyMOL: A communications tool for computational models. *Abstracts of Papers of the American Chemical Society* **230**, U1371–U1372 (2005).
49. Dominy, C. N. & Andrews, D. W. Site-directed mutagenesis by inverse PCR. *Methods Mol Biol* **235**, 209–23 (2003).

Acknowledgements

We are grateful to the Biomedical Research Council of Singapore (BMRC), A*STAR, (R154000461305) and AcRF (Tier 1) (R154000563112) National University of Singapore (NUS), for the partial support of this study. TRC and YX are supported by NIH grant NS053422. X-ray diffraction data for this study were measured at beamline X6A National Synchrotron Light Source (NSLS), BNL New York, USA. VPRC is a graduate scholar in receipt of a research scholarship from the NUS.

Author contributions

J.S. conceived of the study. V.P.R.C. carried out crystallographic, mutational and I.T.C. experiments. V.P.R.C. and J.Se. analyzed the X-ray data. Y.X. and T.R.C. performed and analyzed electrophysiology experiments. V.P.R.C. and J.S. wrote the manuscript.

Additional information

Supplementary information accompanies this paper at http://www.nature.com/scientificreports

Competing financial interests: The authors declare no competing financial interests.

How to cite this article: Chichili, V.P.R., Xiao, Y.C., Seetharaman, J., Cummins, T.R. & Sivaraman, J. Structural Basis for the Modulation of the Neuronal Voltage-Gated Sodium Channel $Na_V1.6$ by Calmodulin. *Sci. Rep.* **3**, 2435; DOI:10.1038/srep02435 (2013).